Electrochemistry

Deutsche Ausgabe: DOI: 10.1002/ange.201605926
Internationale Ausgabe: DOI: 10.1002/anie.201605926

The Origin of Improved Electrical Double-Layer Capacitance by Inclusion of Topological Defects and Dopants in Graphene for Supercapacitors

Jiafeng Chen[+], Yulei Han[+], Xianghua Kong, Xinzhou Deng, Hyo Ju Park, Yali Guo, Song Jin, Zhikai Qi, Zonghoon Lee, Zhenhua Qiao, Rodney S. Ruoff,* and Hengxing Ji**

Abstract: *Low-energy density has long been the major limitation to the application of supercapacitors. Introducing topological defects and dopants in carbon-based electrodes in a supercapacitor improves the performance by maximizing the gravimetric capacitance per mass of the electrode. However, the main mechanisms governing this capacitance improvement are still unclear. We fabricated planar electrodes from CVD-derived single-layer graphene with deliberately introduced topological defects and nitrogen dopants in controlled concentrations and of known configurations, to estimate the influence of these defects on the electrical double-layer (EDL) capacitance. Our experimental study and theoretical calculations show that the increase in EDL capacitance due to either the topological defects or the nitrogen dopants has the same origin, yet these two factors improve the EDL capacitance in different ways. Our work provides a better understanding of the correlation between the atomic-scale structure and the EDL capacitance and presents a new strategy for the development of experimental and theoretical models for understanding the EDL capacitance of carbon electrodes.*

EDL capacitors, also called supercapacitors, store energy by forming an EDL at the electrolyte–electrode interface.[1] The separation distance of charges at the EDL is <1 nm and the electrodes are typically made of porous carbon with a high specific surface area (SSA) of $>1500\ m^2 g^{-1}$, due to which exceptionally large power densities and long cyclic lifetimes are possible.[2] Nevertheless, the operation mechanism of the EDL capacitors results in a gravimetric energy that is one order of magnitude lower than that of a battery, which greatly limits their applications.[3] The major strategies to improve the EDL capacitance of carbon materials include: 1) Optimizing the pore structure in carbon to allow only the desolvated ions to penetrate, thereby reducing the charge separation distance of the EDL;[4] (2) increasing the SSA to enhance the active area of the EDL;[5] and (3) introducing dopants, for example, nitrogen (N) atoms or creating topological defects[6] to improve the capacitance per unit area of the EDL. Recently, the configuration of the nitrogen dopant in graphene was identified as critical to the electrocatalytic activity for the oxygen reduction reaction.[7] Similarly, an in-depth understanding of the mechanisms through which the topological defects and dopants may affect the EDL is demanded for the rational design of electrode materials.

To study the combined influence of the topological defects and dopants on the EDL capacitance, several requirements need to be fulfilled due to the complexity of the carbon and dopant structure. First, the defect and/or dopant concentration has to be precisely controlled, and this should be combined with a reliable measurement of the configuration of the defect and dopant. Second, the interfacial area between the electrolyte and the porous electrode should be accurately measured. Third, electrodes of identical micropore structure and porosity but with different concentrations of defect and/or dopant need to be made and compared. However, this is rather difficult to achieve for electrodes prepared by mixing carbon powders with binders followed by rolling because of their complex and porous structures and the unpredictable wettability of such electrodes.

[*] J. F. Chen,[+] Y. L. Guo, S. Jin, Z. K. Qi, Prof. H. X. Ji
Department of Materials Science and Engineering, CAS Key Laboratory of Materials for Energy Conversion, iChEM (Collaborative Innovation Center of Chemistry for Energy Materials)
University of Science and Technology of China
Hefei, Anhui 230026 (China)
E-mail: jihengx@ustc.edu.cn

Y. L. Han,[+] X. Z. Deng, Prof. Z. H. Qiao
ICQD, Hefei National Laboratory for Physical Sciences at Microscale, Synergetic Innovation Center of Quantum Information and Quantum Physics, CAS Key Laboratory of Strongly-Coupled Quantum Matter Physics, and Department of Physics
University of Science and Technology of China
Hefei, Anhui 230026 (China)
E-mail: qiao@ustc.edu.cn

Prof. X. H. Kong
School of Chemistry and Chemical Engineering
Hefei University of Technology
Hefei, Anhui 230009 (China)

H. J. Park, Prof. Z. Lee, Prof. R. S. Ruoff
School of Materials Science and Engineering, Ulsan National Institute of Science and Technology (UNIST)
Ulsan 44919 (Republic of Korea)

Prof. Z. Lee, Prof. R. S. Ruoff
Center for Multidimensional Carbon Materials
Institute for Basic Science Center at UNIST Campus
Ulsan 44919 (Republic of Korea)
E-mail: ruofflab@gmail.com

[+] These authors contributed equally to this work.

Supporting information and the ORCID identification number(s) for the author(s) of this article can be found under: http://dx.doi.org/10.1002/anie.201605926.

We overcame these obstacles by using planar electrodes based on single-layer graphene synthesized by chemical vapor deposition (CVD). The theoretically estimated SSA of approximately 1310 $m^2 g^{-1}$ of the CVD graphene with one side exposed to the electrolyte is similar to that of the highly porous carbon powders used in practical EDL capacitors (ca. 1500 $m^2 g^{-1}$). The CVD graphene has a thickness of one atomic-layer, which is the lower limit of the wall thickness of the micropores in highly porous carbon powders.[8] The planar electrode geometry ensures a reliable measurement of the area of the interface between the electrolyte and the graphene electrode. We measured the EDL capacitance and calculated the quantum capacitance of two series of graphene electrodes containing either topological defects or N-dopants in different concentrations. The experimental and theoretical studies show that the topological defects improve the density of states (DOS) and the N-dopants can tune the Fermi-level of graphene, both of which significantly influence the quantum capacitance that is connected in series with the Helmholtz capacitance and therefore modify the EDL capacitance.

The single-layer graphene was synthesized by CVD (Supporting Information, Figure S1), and the electrode was prepared by transferring the graphene sheet to a polyethylene terephthalate (PET) substrate (see Experimental Section in the Supporting Information, and Figure 1 a). We tested the stability of the graphene electrode by comparing the scanning electron microscopy (SEM) image and the cyclic voltammetry (CV) curves of the electrode before and after 40 min of capacitance measurement. Figure S1, in the Supporting Information, shows that the morphology and the CV curves remained unchanged, which demonstrates the structural and electrochemical stability of CVD graphene under the conditions of the capacitance measurement. The CV signals (Supporting Information, Figure S1 e) due to either a Faradaic reaction or ion-specific adsorption are not detected, which indicates that the observed current is mainly due to the charging/discharging of the EDL at the graphene/electrolyte interface.

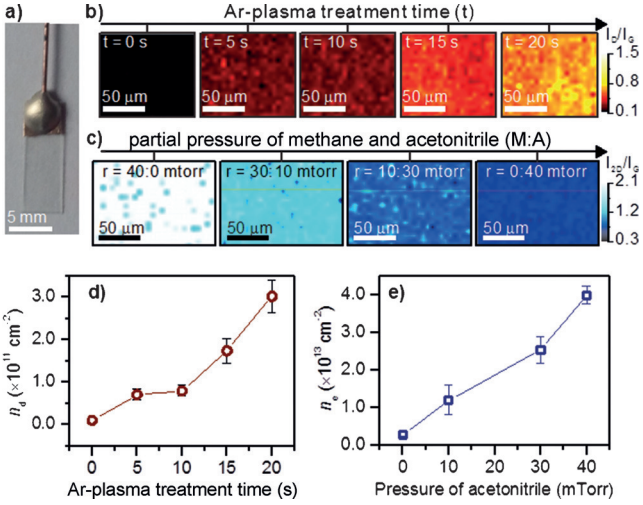

Figure 1. a) Photograph of the electrode prepared from single-layer graphene. b) Raman maps drawn from the I_D/I_G of the Ar^+ plasma-treated graphene and c) from the I_{2D}/I_G of the N-doped graphene. d) The defect concentration (n_d) and e) the charge carrier density (n_e) of graphene electrodes.

We prepared two series of graphene electrodes containing different concentrations of either topological defects or N-dopants. The topological defects were introduced by exposing graphene to Ar^+ plasma, and the defect concentration was varied by controlling the exposure time (Figure 1 b). Raman mapping was performed on each sample at five different regions to acquire approximately 10000 Raman spectra, and the average intensity ratio of the D band to the G band (I_D/I_G) was calculated to quantify the Ar^+ plasma-induced topological defect concentration (see the Supporting Information, Experimental Section and Figure S2).[9] The small variation of the I_D/I_G values measured in different regions of the sample confirms the uniform defect concentration (at the scale of the Raman spot size; Figure 1 b). N-doped graphene was prepared by CVD at different partial pressures of acetonitrile (Supporting Information, Table S1). The X-ray photoelectron spectrum (XPS) is able to detect the N-dopant concentration of 4.0 at% for graphene synthesized with pure acetonitrile precursor, but it is rather challenging to quantify the atomic ratios of N-dopants for doped graphene synthesized using a mixture of methane and acetonitrile, due to the low signal-to-noise ratio in XPS for the N species when doped in single-layer graphene. Electrical measurements have shown that the N-doped graphene has a negatively doped electronic behavior,[10] and the sensitivity of the Raman spectrum to the charge-carrier density has also been reported.[11] Therefore, it was possible to calculate the charge-carrier densities of the doped graphene sheets synthesized with different partial pressures of acetonitrile from the average values of I_{2D}/I_G (Figure 1 c and the Supporting Information, Figure S3).[12]

In Figure 1 d, we show the defect concentration (n_d) of a graphene sample that was exposed stepwise to Ar^+ plasma for 5 s at each step with an accumulated exposure time of 20 s. The accumulated defect concentration increases to $n_d = (3.0 \pm 0.4) \times 10^{11}$ cm^{-2}, which is about 30-fold higher than that for pristine graphene ($n_d = (0.10 \pm 0.06) \times 10^{11}$ cm^{-2}). The non-linear increase of n_d at the second round of Ar^+ plasma treatment (10 s) is not clearly understood at present. The charge carrier density (n_e) of the N-doped graphene shows an almost linear increase with the partial pressure of acetonitrile (Figure 1 e). The maximum n_e is $(4.0 \pm 0.2) \times 10^{13}$ cm^{-2} for graphene synthesized with pure acetonitrile, which is about 14-fold higher than for pristine graphene, $n_e = (0.28 \pm 0.06) \times 10^{13}$ cm^{-2}.

The EDL capacitances (C_{EDL}) of the graphene electrodes with different concentrations of topological defects and N-dopant levels were measured by electrochemical impedance spectroscopy (EIS; Figures S4 and S5). Notably, the C_{EDL} in Figure 2 is a differential capacitance as the values were acquired at a fixed potential when sweeping the frequency. The C_{EDL} of pristine graphene as a function of the potential (V_{EDL}, with respect to the potential of a standard hydrogen electrode (SHE)) shows a concave shape with a minimum of 1.0 μF cm^{-2}. After EIS measurement, the pristine graphene was treated by Ar^+ plasma for five seconds to measure the

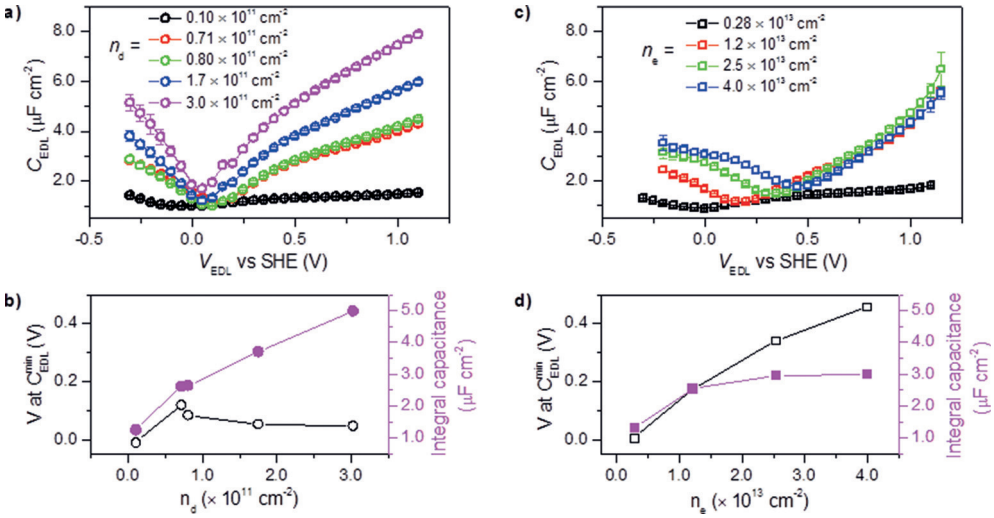

Figure 2. a) Differential EDL capacitance of a graphene electrode with different topological defect concentrations. b) The potential of the capacitance minimum and the integral capacitance derived from the C_{EDL}–V_{EDL} curves in (a). c) Differential EDL capacitance of the electrodes prepared from single-layer graphene synthesized at various acetonitrile partial pressures. d) The potential of the capacitance minimum and the integral capacitance derived from the C_{EDL}–V_{EDL} curves in (c). The error bars in (a) and (c) show the standard error of the mean for the measured impedance values.

C_{EDL} of the graphene with defects before the next round of plasma treatment and EIS measurement. The C_{EDL}–V_{EDL} curves for graphene with defects also show concave shapes (Figure 2a). The rate of increase in C_{EDL} with increasing potential, rises significantly as a function of the defect concentration. This increase is accompanied by an increase of C_{EDL} minimum to 1.7 μF cm^{-2}. Therefore, the integral capacitance evaluated from the area between the C_{EDL}–V_{EDL} curve and the x-axis at $C_{EDL} = 0$ within a potential window of −0.3 to 1.1 V increases almost linearly and reaches a fourfold increase after Ar^+ plasma treatment for an accumulated time of 20 s (Figure 2b). However, the potential of the C_{EDL} minimum is slightly up-shifted to 0.05 V (Figure 2b), which implies a negligible charge doping of the graphene sheets due to defects.

The concave-shaped curves observed for graphene with N-dopants (Figure 2c) are different from those observed for the defective graphene. The increases in the rates of the EDL capacitance with increasing electrode potential are almost identical for the N-doped graphene samples (see red, blue, and green curves in Figure 2c), and the potential corresponding to the C_{EDL} minimum increases almost linearly to 0.46 V with increase in doping level (Figure 2d) even though the value of the C_{EDL} minimum upshifts to 1.78 μF cm^{-2}, similar to the defective graphene (Figures 2a). This relative shift of the C_{EDL} minimum to a higher applied potential originates from the negative charge doping due to the introduction of N-dopants.[10] These changes lead to a gradual increase in the integral capacitance with increased N-doping concentration, before leveling off for charge-carrier concentrations larger than 2.5×10^{13} cm^{-2} (Figure 2d).

The experimentally measured C_{EDL} values show a strong correlation with the topological defects or the N-dopants; however, the dependence of the C_{EDL} on the potential is different for these two types of defects. Previous reports have explained the dopant-induced increase in capacitance by invoking the space-charge capacitance,[8,13] which, in series with a Helmholtz capacitance (C_H), represents the spread of the induced electrode-charge into the bulk and is dependent on the extent of charge doping. However, in Figure 2, we show that the C_{EDL} minimum of graphene with topological defects is at the same potential of zero charge, indicating that there is negligible charge doping, and the electrode has only one atomic-layer, thereby implying that the observed capacitance increase cannot be attributed to the space-charge capacitance. Moreover, a contribution from a possible pseudo-capacitance is unlikely in our case, since no Faradaic reaction is detected in the CV curves (Supporting Information, Figure S1). In this context, we have referred to an earlier work in which the quantum capacitance (C_Q) accounting for the low density of states (DOS) in low-dimensional materials (for example, graphene) was added in series with C_H to explain the limits in the areal C_{EDL} values for highly porous carbon materials.[14]

To get a deeper understanding of the measured C_{EDL} in these defective or doped graphene systems, we estimated the C_Q of graphene containing either topological defects or N-dopants from first-principles calculations and the tight-binding method. Considering previous theoretical findings and our numerical estimation that the Stone–Wales defect has a formation energy that is approximately 2.7 eV lower than for the monovacancy and the divacancy (Supporting Information, Figure S6),[15] we conclude that the Stone–Wales type topological defect is the most probable defect formed when graphene is exposed to Ar^+ plasma (Figure 3a). Therefore, in Figure 3b, we show the potential dependence of the C_Q of graphene at different concentrations of Stone–Wales defects. We observe that the C_Q minimum slightly increases but is mostly at a potential close to zero for the different defect concentrations. At potential values far from zero, C_Q increases with the defect concentration. This behavior for C_Q is very similar to the experimentally observed C_{EDL} (Figure 2a). We also find that the Stone–Wales defects can significantly improve the DOS of graphene near the Fermi-level (Supporting Information, Figure S6) and hence the C_Q. To further test our conclusion, we examined the defect structure of the Ar^+ plasma-treated graphene sheet by transmission electron microscopy (TEM). We found that the

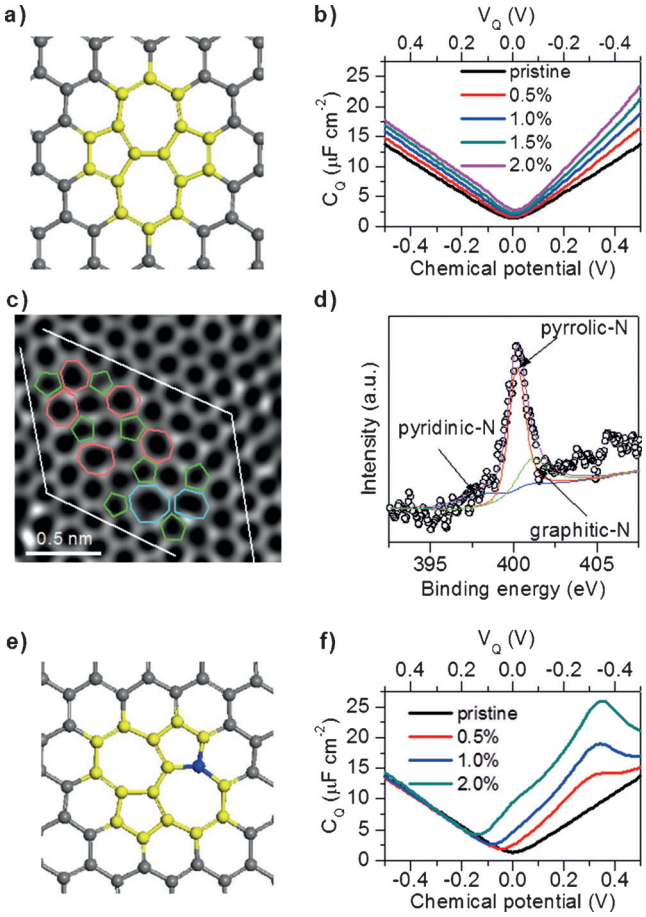

Figure 3. a) Schematic of the Stone–Wales defect. b) Quantum capacitance of graphene with Stone–Wales defects in different concentrations. c) TEM image of single-layer graphene after exposure to Ar^+ plasma for 15 s. Red = heptagon, green = pentagon, and blue = octagon. White lines indicate the location of the hexagons. d) XPS of N-doped graphene synthesized with acetonitrile. e) Schematic of the pyrrolic-N doped in the graphene lattice. Blue = N. f) Quantum capacitance of graphene with different concentrations of pyrrolic-N. V_Q is the bias applied to the C_Q.

heptagon–pentagon pairs are the dominant defect structures besides a few octagons, and the surrounding hexagons have the same orientation (Figure 3c), indicating that the Stone–Wales-like topological defects are not located at the graphene grain boundaries but are created during Ar^+ plasma treatment and should be the reason for the enhancement of C_Q.

The XPS of the N-doped graphene shows an intense peak at a binding energy of 400.2 eV (Figure 3d), which indicates that most of the nitrogen is pyrrolic.[16] One probable configuration of pyrrolic-N is a pentagon composed of four C atoms with one N-atom connecting with two neighboring C atoms in a circle.[16a] The TEM study by Arenal et al. showed that the pyrrolic-N having an energy loss of 400 eV in the electron energy loss spectrum is connected to a Stone–Wales defect to form C–N bonds linked to three C atoms (Figure 3e).[17] We considered graphene with these two types of pyrrolic-N and calculated their DOS and formation energy (Supporting Information, Figure S7). We chose the three-coordinated pyrrolic-N configuration to numerically calculate the corresponding C_Q because it negatively dopes the graphene and the formation energy is lower. In Figure 3f, the chemical potential corresponding to the C_Q minimum down-shifts significantly, which can be attributed to the up-shift of the Fermi-level as a result of the negative charge doping. Therefore, a positive bias (V_Q) on the graphene electrode is needed to reach the C_{EDL} minimum. We tried to observe the configuration of the N-dopants by TEM. Unfortunately, the small difference in atomic numbers between the N and C atoms makes it challenging to identify the N-dopants. Nevertheless, our first-principles and tight-binding calculations qualitatively explain that the Stone–Wales defects enhance the DOS and the pyrrolic N-dopants up-shift the Fermi-level of the system, both of which significantly affect the C_Q connected in series with the C_H.

Pioneering theoretical work also demonstrated that the defects and dopants affect the C_{EDL} by tuning the C_Q of graphene, which originates from the change of the graphene band structure.[18] Our experimental measurements and calculations, based on these previous theoretical work, suggest that although the changes in C_{EDL} that arise from both the topological defects and N-dopants have the same origin of C_Q, the microscopic mechanisms responsible for this improvement are different in these two approaches. The practical gravimetric capacitance is an integral of the measured differential C_{EDL} over V_{EDL} (Figure 2). This value can be evaluated from the area (shown in green in Figure 4a) between the C_{EDL}–V_{EDL} curve and the x-axis at $C_{EDL} = 0$ within a potential width of approximately 1 V (this is defined by the hydrogen and oxygen evolution potentials of the aqueous electrolyte). The topological defect significantly increases the changing rate of the C_{EDL} with the V_{EDL} as

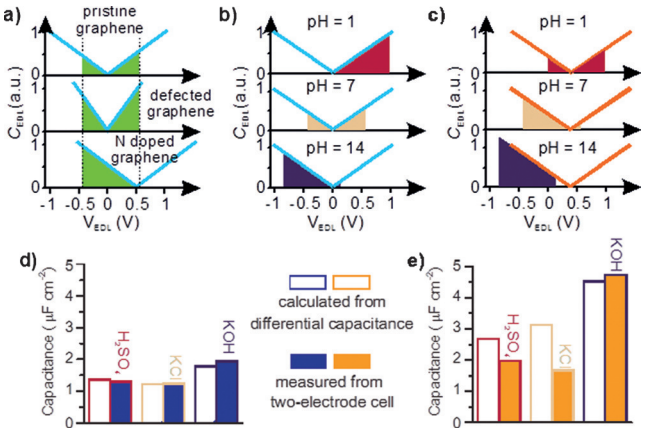

Figure 4. a) Schematic of the EDL capacitance of pristine, defective, and N-doped graphene in the same potential window. Schematic of the EDL capacitance of b) the pristine graphene and c) the N-doped graphene with different potential windows. The color and area under the C_{EDL}–V_{EDL} present the pH and the integral capacitance value, respectively. The integral capacitances of d) the pristine graphene and e) the N-doped graphene that were calculated from the C_{EDL}–V_{EDL} curve in different potential windows and that were measured with a two-electrode cell with 1 M H_2SO_4, KCl, and KOH. The hollow bars present the calculated values from the C_{EDL}–V_{EDL} curve, and the solid bars present the measured values of a two-electrode cell of both the positive and negative electrodes made from single-layer graphene.

a result of the improved DOS, thereby increasing the integral capacitance. The N-dopant-induced charge-doping does not significantly change the DOS, but can shift the Fermi-level, and hence the C_{EDL} minimum moves closer to the edge of the potential window, which leads to a significant increase in the integral capacitance. A quantitative comparison between the measured C_{EDL} and the calculated C_Q is not possible due to the limitations of the experimental technique in measuring the defect and dopant concentration (Supporting Information, Section 4).

Nevertheless, this mechanism may shed light on the capacitance differences between two-electrode cells with acidic, neutral, and alkaline aqueous electrolytes that have been reported in the literature.[19] The potential window with respect to SHE of a two-electrode supercapacitor cell with aqueous electrolyte is a function of pH.[20] The differential C_{EDL} minimum for a pure graphene electrode is at approximately 0 V with respect to SHE, that is, almost at the center of the potential window in a neutral (pH 7) electrolyte, yet is close to the edge of the potential window in an acidic (pH 1) or alkaline (pH 14) electrolyte (Figure 4b), thus the integral capacitance obtained with a neutral electrolyte is smaller than those measured with acidic and alkaline electrolytes. We calculated the integral capacitance of the pristine graphene by the C_{EDL}–V_{EDL} curve. The calculated integral capacitances (hollow bars in Figure 4d) in the potential window of −0.5 to +0.5 V (neutral) with respect to SHE are 88% and 68% of those calculated in the potential window of 0 to +1.0 V (acidic) and the potential window of −1.0 to 0 V (alkaline), respectively. We measured the area-normalized capacitances by CV (Supporting Information, Figure S9) of a two-electrode cell with both the positive and negative electrodes made from single-layer graphene (without plasma treatment or N-dopants) in 1M H_2SO_4, KCl, and KOH. The electrodes were not changed when replacing the electrolytes. The capacitance measured in KCl solution is 95% and 65% of those measured in H_2SO_4 and KOH solution, respectively (solid bars in Figure 4d). As the N-dopants shift the potential of the C_{EDL} minimum to a higher value (Figure 2c), the integral capacitance of N-doped graphene would be higher in the alkaline electrolyte (Figure 4c). The calculated values from the C_{EDL}–V_{EDL} curve are 2.5, 3.1, and 4.5 $\mu F\,cm^{-2}$ (hollow bars in Figure 4e), respectively, in the potential windows of 0 to +1.0 V (acidic), −0.5 to +0.5 V (neutral), and −1.0 to 0 V (alkaline). The capacitances measured by CV with a two-electrode cell composed of N-doped graphene electrodes are 2.0, 1.7, and 4.8 $\mu F\,cm^{-2}$ (solid bars in Figure 4e) in 1M H_2SO_4, KCl, and KOH solutions, respectively. In the above discussion, we have mainly concentrated on the effect of the topological defects and dopants in carbon, which is to change the quantum capacitance and to thereby enhance the EDL capacitance. However, the potential window of an electrochemical cell is determined not only by the electrolyte, but also the electrode. The above potential window used for calculating the integral capacitance may not match that of the two-electrode cell. The EDL capacitance of carbon electrodes, especially those prepared by carbon powders, in a supercapacitor depends on a complex interplay of different factors, such as the wettability, micropore size, chemical composition, the level of graphitization of the carbon, and the electrolyte.

In summary, we investigated the role of topological defects and N-dopants on the EDL capacitance by using single-layer graphene electrodes with controlled defect and N-dopant concentrations. The topological defects improve the DOS and the N-dopants can tune the Fermi-level of graphene, both of which significantly influence the quantum capacitance that is connected in series with the Helmholtz capacitance, and which therefore modify the EDL capacitance. These findings provide insights into the influence of the quantum effect on macroscopic properties such as the EDL capacitance in nanomaterials and low dimensional materials. This could in turn play an important role in designing better supercapacitors with optimized carbon electrodes in future applications.

Acknowledgements

We appreciate funding support from the National Natural Science Foundation of China (21373197, 11474265 and 21503064), 100 Talents Program of the Chinese Academy of Sciences, the China Government Youth 1000-Plan Talent Program, Fundamental Research Funds for the Central Universities (KY2060140025, WK2060140003, WK3510000001, and WK2030020027), and the National Key R & D Program (Grant No. 2016YFA0301700). The Supercomputing Center of USTC is gratefully acknowledged for high-performance computing assistance. Z.L. and R.S.R. appreciate support from the Institute for Basic Science (Grant IBS-R019-D1).

Keywords: electrical double-layers · nitrogen dopants · quantum capacitance · single-layer graphene · topological defects

How to cite: *Angew. Chem. Int. Ed.* **2016**, *55*, 13822–13827
Angew. Chem. **2016**, *128*, 14026–14031

[1] B. E. Conway, *J. Electrochem. Soc.* **1991**, *138*, 1539.
[2] J. R. Miller, P. Simon, *Science* **2008**, *321*, 651–652.
[3] a) P. Simon, Y. Gogotsi, *Nat. Mater.* **2008**, *7*, 845–854; b) M. F. El-Kady, M. Ihns, M. Li, J. Y. Hwang, M. F. Mousavi, L. Chaney, A. T. Lech, R. B. Kaner, *Proc. Natl. Acad. Sci. USA* **2015**, *112*, 4233–4238; c) Z. Yang, J. Ren, Z. Zhang, X. Chen, G. Guan, L. Qiu, Y. Zhang, H. Peng, *Chem. Rev.* **2015**, *115*, 5159–5223.
[4] C. Largeot, C. Portet, J. Chmiola, P. L. Taberna, Y. Gogotsi, P. Simon, *J. Am. Chem. Soc.* **2008**, *130*, 2730–2731.
[5] W. Gu, G. Yushin, *Wiley Interdisc. Rev.: Energy Environ.* **2014**, *3*, 424–473.
[6] a) J. Zhou, J. Lian, L. Hou, J. Zhang, H. Gou, M. Xia, Y. Zhao, T. A. Strobel, L. Tao, F. Gao, *Nat. Commun.* **2015**, *6*, 8503; b) M. A. Pope, I. A. Aksay, *J. Phys. Chem. C* **2015**, *119*, 20369–20378.
[7] D. Guo, R. Shibuya, C. Akiba, S. Saji, T. Kondo, J. Nakamura, *Science* **2016**, *351*, 361–365.
[8] O. Barbieri, M. Hahn, A. Herzog, R. Kötz, *Carbon* **2005**, *43*, 1303–1310.
[9] M. M. Lucchese, F. Stavale, E. H. M. Ferreira, C. Vilani, M. V. O. Moutinho, R. B. Capaz, C. A. Achete, A. Jorio, *Carbon* **2010**, *48*, 1592–1597.

[10] D. Wei, Y. Liu, Y. Wang, H. Zhang, L. Huang, G. Yu, *Nano Lett.* **2009**, *9*, 1752 – 1758.
[11] C. Ferrari, *Solid State Commun.* **2007**, *143*, 47 – 57.
[12] A. Das, S. Pisana, B. Chakraborty, S. Piscanec, S. K. Saha, U. V. Waghmare, K. S. Novoselov, H. R. Krishnamurthy, A. K. Geim, A. C. Ferrari, A. K. Sood, *Nat. Nanotechnol.* **2008**, *3*, 210 – 215.
[13] H. Gerischer, R. McIntyre, D. Scherson, W. Storck, *J. Phys. Chem.* **1987**, *91*, 1930 – 1935.
[14] a) H. Ji, X. Zhao, Z. Qiao, J. Jung, Y. Zhu, Y. Lu, L. L. Zhang, A. H. MacDonald, R. S. Ruoff, *Nat. Commun.* **2014**, *5*, 3317; b) J. Xia, F. Chen, J. Li, N. Tao, *Nat. Nanotechnol.* **2009**, *4*, 505 – 509.
[15] Z. F. Hou, X. L. Wang, T. Ikeda, K. Terakura, M. Oshima, M. Kakimoto, S. Miyata, *Phys. Rev. B* **2012**, *85*, 165439.
[16] a) H. Terrones, R. Lv, M. Terrones, M. S. Dresselhaus, *Rep. Prog. Phys.* **2012**, *75*, 062501; b) T. Susi, T. Pichler, P. Ayala, *Beilstein J. Nanotechnol.* **2015**, *6*, 177 – 192.
[17] R. Arenal, K. March, C. P. Ewels, X. Rocquefelte, M. Kociak, A. Loiseau, O. Stephan, *Nano Lett.* **2014**, *14*, 5509 – 5516.
[18] a) E. Paek, A. J. Pak, K. E. Kweon, G. S. Hwang, *J. Phys. Chem. C* **2013**, *117*, 5610 – 5616; b) A. J. Pak, E. Paek, G. S. Hwang, *Carbon* **2014**, *68*, 734 – 741; c) B. C. Wood, T. Ogitsu, M. Otani, J. Biener, *J. Phys. Chem. C* **2014**, *118*, 4 – 15; d) G. M. Yang, H. Z. Zhang, X. F. Fan, W. T. Zheng, *J. Phys. Chem. C* **2015**, *119*, 6464 – 6470.
[19] a) K. Torchała, K. Kierzek, J. Machnikowski, *Electrochim. Acta* **2012**, *86*, 260 – 267; b) M. P. Bichat, E. Raymundo-Piñero, F. Béguin, *Carbon* **2010**, *48*, 4351 – 4361; c) H. Wang, Y. Wang, Z. Hu, X. Wang, *ACS Appl. Mater. Interfaces* **2012**, *4*, 6827 – 6834; d) J.-W. Lang, X.-B. Yan, W.-W. Liu, R.-T. Wang, Q.-J. Xue, *J. Power Sources* **2012**, *204*, 220 – 229.
[20] J. Bard, L. R. Faulkner, *Electrochemical Methods: Fundamentals and Applications*, 2nd ed., Wiley, New York, **2000**.

Received: June 19, 2016
Revised: August 5, 2016
Published online: October 4, 2016

